JACS
JOURNAL OF THE AMERICAN CHEMICAL SOCIETY
Article
pubs.acs.org/JACS

Proton-Based Structural Analysis of a Heptahelical Transmembrane Protein in Lipid Bilayers

Daniela Lalli,[†] Matthew N. Idso,[‡] Loren B. Andreas,[†,∥] Sunyia Hussain,[‡] Naomi Baxter,[§] Songi Han,[‡,§] Bradley F. Chmelka,*[,‡] and Guido Pintacuda*[,†]

[†]Centre de RMN à Très Hauts Champs, Institut des Sciences Analytiques (UMR 5280 - CNRS, ENS Lyon, UCB Lyon 1), Université de Lyon, 69100 Villeurbanne, France

[‡]Department of Chemical Engineering, University of California, Santa Barbara, California 93106, United States

[§]Department of Chemistry and Biochemistry, University of California, Santa Barbara, California 93106, United States

Supporting Information

ABSTRACT: The structures and properties of membrane proteins in lipid bilayers are expected to closely resemble those in native cell-membrane environments, although they have been difficult to elucidate. By performing solid-state NMR measurements at very fast (100 kHz) magic-angle spinning rates and at high (23.5 T) magnetic field, severe sensitivity and resolution challenges are overcome, enabling the atomic-level characterization of membrane proteins in lipid environments. This is demonstrated by extensive ^{1}H-based resonance assignments of the fully protonated heptahelical membrane protein proteorhodopsin, and the efficient identification of numerous ^{1}H−^{1}H dipolar interactions, which provide distance constraints, inter-residue proximities, relative orientations of secondary structural elements, and protein−cofactor interactions in the hydrophobic transmembrane regions. These results establish a general approach for high-resolution structural studies of membrane proteins in lipid environments via solid-state NMR.

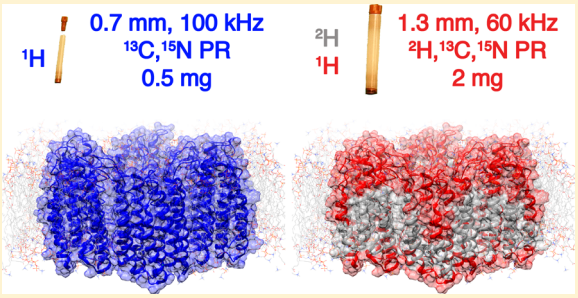

INTRODUCTION

Atomic level characterization of membrane proteins in lipid bilayers is essential for understanding their functions, although extremely challenging. Membrane proteins in lipid environments generally lack long-range order, and tumble slowly in solutions, which respectively render scattering investigations infeasible and jeopardize liquid-state NMR investigations. Magic-angle spinning (MAS) solid-state NMR spectroscopy is a powerful tool that can reveal both structural and dynamical details of such systems,[1] yet its application has been limited by low spectral sensitivity and resolution, as well as by the difficulty in obtaining large (~20 mg) quantities of isotopically labeled proteins.

Many strategies have been employed to overcome the resolution and sensitivity issues that impede structural characterization of membrane proteins by MAS NMR. Proton detection is a powerful technique that exploits the high gyromagnetic ratio and abundance of proton nuclei to enhance the spectral sensitivity.[2] However, despite encouraging proof-of-principle studies performed on fully protonated model systems,[3] applications of ^{1}H-detection to membrane proteins in native-like lipid environments have been hindered by the low ^{1}H spectral resolution under moderate MAS rates (<40 kHz). Higher spectral resolution[4] can be achieved in part by proton dilution strategies (typically perdeuteration and back-protonation at the exchangeable sites) to quench the ^{1}H−^{1}H dipolar couplings that broaden NMR signals.[5] This strategy, however, is problematic during protein expression, due to anemic growth in deuterium oxide which sometimes is even incompatible with protein expression, as for example in mammalian cells. When feasible, it allows reintroduction of ^{1}H species exclusively at sites that are exchangeable and accessible to solvent, which notably do not include the extensive hydrophobic transmembrane regions, thereby precluding their analyses by ^{1}H-detected spectroscopy.[6] Unfolding and refolding membrane proteins leads to the introduction of ^{1}H species at the exchangeable sites of transmembrane regions, however such protocols are not general, and specific examples are rare.[1l,5d,7] To address this in part, isotopic labeling strategies have been developed in which membrane proteins are expressed in H_2O in the presence of deuterated ^{13}C glucose, such that ^{1}H/^{2}H species are homogeneously distributed in both water-accessible and inaccessible regions.[8] Nevertheless, in such cases the ^{1}H/^{2}H isotopomeric distributions often result in poorly resolved ^{13}C resonances from side-chain moieties that are crucial for structure determination.

The advent of MAS NMR probes capable of spinning at rates of 100 kHz or greater has reduced the amount of sample required,[2,5e,f,9] and, most importantly, reduced the need for

Received: May 24, 2017
Published: July 20, 2017

DOI: 10.1021/jacs.7b05269
J. Am. Chem. Soc. 2017, 139, 13006−13012

proton dilution.[10] This has opened unprecedented opportunities for structural investigations of biosolids by using sensitive ^{1}H-detected methods,[10,11] with a dramatic reduction in homogeneous line broadening to improve the resolution of ^{1}H resonances. However, even at the fastest (~100 kHz) sample spinning rates and the highest magnetic fields (23.5 T) currently available, membrane proteins in lipid bilayers remain challenging to study by NMR (or other methods), because of their inherently heterogeneous lipid bilayer environments in which they are naturally diluted and which limit spectral resolution and signal sensitivity.

Transmembrane proteins, in particular, are incorporated into lipid bilayers and perform sensing, transport and enzymatic functions in support of cellular viability. One example is the green variant of proteorhodopsin, a light-activated H^+-ion pump of 240 residues that in solution has an archetypical heptahelical transmembrane protein structure with a retinal cofactor.[12] While the structure of monomeric proteorhodopsin in detergents has been determined by solution NMR (pdb code: 2L6X),[13] the structure of the protein in native-like lipid environments remains unknown. This is complicated further by the tendency of proteorhodopsin molecules in bilayers to assemble into pentamers and hexamers, which are thought to mediate protein function.[14] Conventional ^{13}C-detected MAS NMR methods have enabled the extensive assignment of backbone and side-chain ^{13}C and ^{15}N resonances of proteorhodopsin oligomers in lipids.[15] However, only a partial assignment of the solvent-exposed amide ^{1}H resonances was possible with ^{1}H-detected measurements on perdeuterated protein, due to incomplete solvent exchange.[6]

Here, we demonstrate very fast (100 kHz) MAS NMR to be a general approach for structural analyses of fully protonated membrane proteins in near-native lipid environments. Notably, we show that the use of fast 100 kHz MAS conditions expedites sequence-specific resonance assignments and facilitates the detection of ^{1}H−^{1}H proximities in hydrophobic transmembrane regions, which are essential features of protein structure and for their function.

EXPERIMENTAL SECTION

Sample Preparation. Expression of isotopically labeled proteorhodopsin was carried out as described by Ward et al.[6] with a few differences. Following overnight growth of *E. coli* cells in the 25 mL culture, the cells were pelleted by centrifugation at ~5000 rpm and resuspended in 75 mL of M9 minimal media with all labels present. Subsequently, the 75 mL culture was grown at 37 °C to an O.D.$_{600}$ of 1.0−1.5 (approximately 6 h) and then added to 925 mL of M9 media (all labels present). Protein expression was induced at an O.D.$_{600}$ of 0.8 by the addition of IPTG to a concentration of 1 mM and allowed to proceed for ~24 h at room temperature without shaking. Protein purification was carried out using methods described previously[14a] with a few modifications. Cells were lysed by a freeze fracture step with three freeze−thaw cycles using liquid nitrogen in addition to probe tip sonication and incubation with DNase, lysozyme, and $MgCl_2$. Then, the large cell fragments containing proteorhodopsin were pelleted by centrifugation at 5000 rpm and then washed with 250 mL of phosphate buffered solution (150 mM KCl and KH_2PO_4, pH ≈ 8.7) by repeatedly suspending the cell pellet in 40 mL of buffer, shaking the solution for 5 min, and pelleting cells by centrifugation. Subsequently, proteorhodopsin was extracted from lysed *E. coli* membranes by overnight incubation of the washed cell fragments in a phosphate buffered solution containing 4% (w/v) *n*-dodecyl-*β*,D-maltoside surfactant. Following the Ni-NTA resin binding, washing and elution steps,[2] the optical purities of the proteorhodopsin samples, as measured by the ratio of absorbances at 280 to 520 nm, typically ranged between 1.8 and 2.2. The concentration of proteorhodopsin was estimated based on the absorbance at 520 nm, using an extinction coefficient of 49 000 $M^{-1}cm^{-1}$. Proteorhodopsin was reconstituted into 1,2-dimyristoyl-*sn*-glycero-3-phosphate (DMPA) and 1,2-dimyristoyl-*sn*-glycero-3-phosphocholine (DMPC) liposomes using procedures described previously, except using a 10 mM HEPES buffer that was titrated to a pH 6.2 using dilute HCl.[15b]

NMR Spectroscopy. All experiments were carried out on a Bruker Avance III 1 GHz standard bore spectrometer operating at a static field of 23.4 T, equipped with a triple channel H, C, N, 0.7 mm probe, at a MAS rate $\omega_r/2\pi$ of 100 kHz. Sample temperature was maintained at about 305 K using a Bruker cooling unit with regulated N_2 gas directed at the rotor. The temperature of this gas measured just before reaching the sample was 280 K. Chemical shifts were referenced to adamantane (^{1}H signal at 1.87 ppm).

The nonselective pulses were set to 1.1 μs at 227 kHz rf-field amplitude (^{1}H), 5.5 μs at 45 kHz rf-field amplitude (^{15}N) and 3.1 μs at 81 kHz rf-field amplitude (^{13}C). The dipolar-based ^{15}N,^{1}H and ^{13}C,^{1}H CP-HSQC experiments (H)CH and (H)NH follow, with little modifications, those introduced by Rienstra and co-workers.[3b,5a] (H)NCAHA, (H)N(CO)CAHA, (H)CANH, (H)(CO)CA(CO)NH, and (H)CONH experiments were performed as described recently.[5d,11b] The irradiation schemes are displayed in Figure S1 of the Supporting Information, SI. The ^{1}H−^{15}N and ^{1}H−^{13}C cross-polarization (CP) were performed using a constant RF frequency applied to ^{15}N and ^{13}C of 40 kHz and a pulse linearly ramped from 90% to 100% of a maximum RF frequency of 130 kHz on ^{1}H. The ^{13}C−^{15}N CP was performed using a constant RF frequency of 60 kHz on ^{13}C and a 10% tangent ramp of 40 kHz on ^{15}N for 10 ms. Low power WALTZ-16 decoupling of 10 kHz was applied for heteronuclear decoupling. Swept low-power TPPM (slTPPM)[16] decoupling was used during ^{13}C, ^{15}N chemical shift evolution with a ^{1}H RF frequency of 25 kHz and a pulse-length duration of 20 μs. DIPSI-2 of $\gamma B_1/2\pi$ = 20 kHz was used for ^{13}C decoupling during acquisition due to the presence of homonuclear ^{13}C−^{13}C *J*-couplings. Suppression of solvent signals[4a] was applied using the MISSISSIPPI scheme[17] without the homospoil gradient for 200 ms. The interscan recycle delay was 1 s.

The (H)CCH experiment follows that reported recently.[10,11b] The composite ^{13}C pulses of 25 kHz were applied for the TOCSY mixing for 15 ms. In the 3D (H)CHH experiment, ^{1}H−^{1}H RFDR recoupling[16] was applied after the back-CP at a ^{1}H RF frequency of 200 kHz, for 1.4 ms. No loss of water from the sample was observed during the acquisition of the spectra. Spectra were apodized in each dimension with 60° to 90° shifted squared sine-bells ("qsine 3" or "qsine 2" in Bruker Topspin), and zero-filled to at least twice the number of points in the indirect dimensions. Where line widths are reported, no apodization was applied for the reported frequencies. Acquisition and processing parameters specific for each data set are summarized in Tables S2. Spectra were processed with Topspin3.5, and their analysis was performed using Cara. The resonance assignments for ^{1}H, ^{13}C, and ^{15}N nuclei are listed in Table S3.

RESULTS AND DISCUSSION

A dipolar-mediated 2D ^{1}H−^{15}N correlation spectrum (Figure 1, blue) of fully protonated U−[^{13}C,^{15}N] proteorhodopsin acquired at 100 kHz MAS shows highly resolved signals from the amide moieties of the protein backbone. These correlations have an average proton line width of 190 Hz fwhm that is significantly narrower than in a spectrum acquired on an identical sample at 60 kHz MAS rates in a 1.3 mm probe (Figure S2). Surprisingly, these spectra show comparable signal sensitivities (Figure S3), despite the significantly lower sample quantity (~0.5 mg, 0.7 mm rotor) at 100 kHz MAS, compared to 60 kHz MAS (~2.0 mg, 1.3 mm rotor). Deuterated proteorhodopsin reprotonated at the amide sites by exchange in 100% protonated buffers, yields enhanced resolution in a ^{1}H−^{15}N correlation spectrum (Figure 1, red) acquired under

DOI: 10.1021/jacs.7b05269
J. Am. Chem. Soc. 2017, 139, 13006−13012

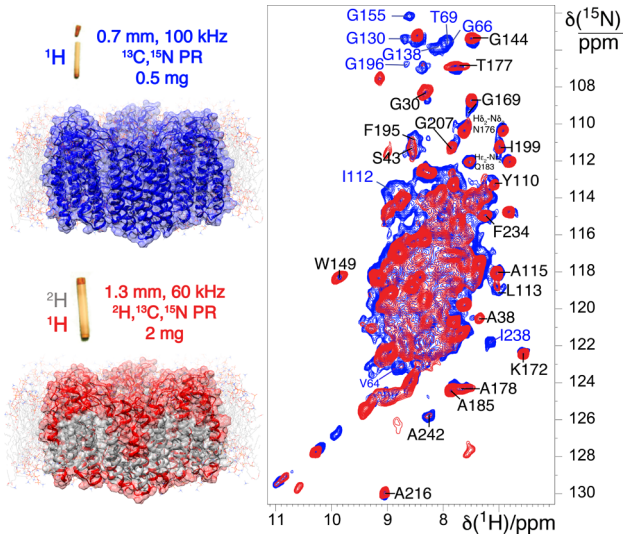

Figure 1. (A) Comparison of 2D ^{1}H−^{15}N CP-HSQC MAS NMR spectra acquired at 305 K on (blue trace) fully protonated U−[^{13}C,^{15}N] proteorhodopsin in DMPC:DMPA lipids at 100 kHz MAS, and (red trace) U−[^{2}H,^{15}N,^{13}C] proteorhodopsin, reprotonated in 100% protonated buffer, in the same lipids at 60 kHz MAS and a field strength of 23.5 T. (B) Schematic diagrams of proteorhodopsin oligomers, modeled from the monomeric protein structure (pdb code: 2L6X, see SI), in which residues with ^{1}H^{N} species are highlighted in blue and red for the fully protonated and perdeuterated samples, respectively.

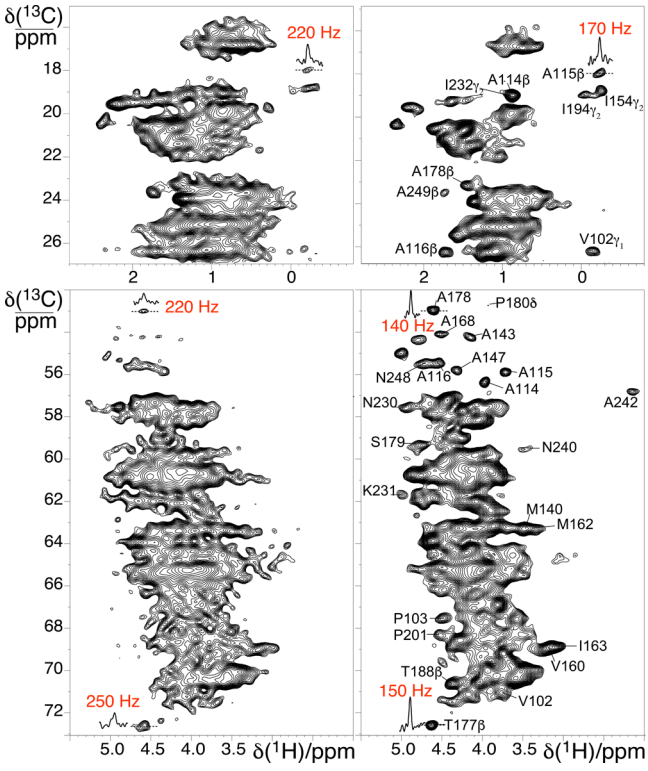

Figure 2. 2D ^{1}H−^{13}C CP-HSQC MAS NMR spectra acquired at 305 K and 23.5 T on fully protonated U−[^{13}C,^{15}N] proteorhodopsin in lipids at MAS rates of 60 kHz (left) and 100 kHz (right). The side chain and alpha regions of the spectra are shown in the top and bottom panels, respectively.

conventional 60 kHz MAS rates, showing average line widths of 140 Hz fwhm. However, the spectrum acquired on the perdeuterated sample at 60 kHz MAS has far fewer cross-peaks (Figure 1, red) than that from the fully protonated (Figure 1, blue) protein at 100 kHz MAS. This reflects an incomplete reintroduction of H^N species in perdeuterated proteorhodopsin, predominantly at residues in the hydrophobic transmembrane regions, which precludes their detection and structural analysis. By comparison, the ubiquity of ^{1}H species in fully protonated proteorhodopsin allows the entire biomolecule to be probed by ^{1}H-detected spectroscopy, in particular moieties on the aliphatic side-chains from which critical structural constraints are derived.

For example, the 2D ^{13}C−^{1}H CP-HSQC spectra of fully protonated proteorhodopsin at 60 kHz (Figure 2, left) and 100 kHz (Figure 2, right) MAS show correlated signals from ^{1}H and ^{13}C nuclei in the side-chains (top panel) and α positions (bottom panel). Substantially enhanced proton resolution is observed under the faster MAS conditions, as established by the larger number of fully resolved correlations that appear only in the spectrum recorded at 100 kHz; these include many ^{1}Hα resonances labeled in Figure 2, bottom panels, as well as ^{1}H methyl resonances (Figure 2, top panels). For several peaks resolved even at 60 kHz, the line widths are observed to be 50−100 Hz broader (Figure 2). The dramatic improvements in resolution enable the use of aliphatic side-chain protons as crucial reporters of protein structure. The significant increase in spectral resolution observed at 100 kHz MAS is surprising. While microcrystalline proteins, capsids, and fibrils often are homogeneous samples with rigid architectures that are amenable to MAS-averaging of homonuclear dipolar interactions, membrane proteins are less homogeneous, comparably flexible, and undergo a range of motions[18] that could reduce the benefits of faster MAS rates in improving signal resolution.

Nevertheless, in spectra from fully protonated proteorhodopsin in lipids, the average ^{1}H line width of ^{15}N−^{1}H correlations from amide moieties is ∼190 Hz fwhm at 100 kHz MAS, compared to ∼280 Hz fwhm at 60 kHz MAS. Greater resolution improvements are observed for aliphatic ^{1}H signals, where average line widths are approximately 145 Hz fwhm at 100 kHz MAS, versus about 235 Hz fwhm estimated from the few resolved signals at 60 kHz. The bulk ^{1}H coherence lifetimes were measured to be 2.5 ms on the fully protonated protein at 100 kHz MAS, which corresponds to residual homogeneous components of ∼125 Hz that suggest inhomogeneous line widths of 155 and 70 Hz for the ^{1}H^{N} and ^{1}Hα signals, respectively. The larger inhomogeneous components for the ^{1}H^{N} species likely arise from a distribution of hydrogen bonding environments, consistent with the larger range of amide ^{1}H^{N} shifts reported generally for proteins in the BMRB. The substantial homogeneous broadening remaining even at 100 kHz MAS conditions indicates that further narrowed ^{1}H line widths could be obtained for faster MAS rates and/or higher magnetic fields.[2,19]

Additionally, the ^{1}H signal resolution of fully protonated proteorhodopsin at 100 kHz MAS is comparable to that obtained with state-of-the-art partial isotopic labeling schemes. These labeling strategies, including fractional deuteration,[5h,20] isoleucine−leucine−valine labeling,[11,21] proton clouds,[5g] and stereospecific array isotopic labeling (SAIL),[22] selectively introduce ^{1}H side-chains into a deuterated protein matrix. Spectra of fully protonated proteorhodopsin in lipids at 100 kHz MAS show 20% higher ^{1}H resolution than for the similar α-helical transmembrane K^+ channel Kcsa in lipid bilayers

DOI: 10.1021/jacs.7b05269
J. Am. Chem. Soc. 2017, 139, 13006−13012

labeled with an inverse fractional deuteration approach and using 60 kHz MAS rates.[8] Importantly, while this labeling scheme yields $^{1}H/^{2}H$ isotopomers that can account for up to 0.3 ppm dispersions in ^{13}C chemical shifts,[23] such effects are negligible in fully protonated proteins probed using 100 kHz MAS.

To facilitate rapid and global sequence-specific resonance assignments, judicious selections of 3D correlation experiments are essential for high sensitivity, in addition to high spectral resolution. Between the two different types of protein backbone ^{13}C species, the coherence lifetimes are longest for $^{13}C'$ species (T_2' = 21 ms, compared to $^{13}C\alpha$ T_2' = 12.5 ms, see Table S1), yielding considerable sensitivity advantages for 3D NMR measurements that rely on evolution of $^{13}C'$ versus $^{13}C\alpha$ coherences. Thus, for sequential resonance assignments of fully protonated proteorhodopsin, we chose the combination of two strategies that leverage the longer lifetimes of the $^{13}C'$ spins by using *J*-mediated $^{13}C'$-$^{13}C\alpha$ coherence transfers[24] and detection of either H^{N}[5d] or Hα resonances.[11b] These two approaches, respectively, use (H)CANH and (H)(CO)CA(CO)NH spectra to correlate signals from $^{1}H-^{15}N$ amide pairs to $^{13}C\alpha$ resonances of adjacent residues, or use (H)NCAHA and (H)N(CO)CAHA to correlate the signals of $^{1}H\alpha-^{13}C\alpha$ pairs to intra and inter-residue ^{15}N species.[11b] Sequential backbone assignments are achieved by simultaneously linking correlations of both $^{1}H-^{15}N$ or $^{1}H\alpha-^{13}C\alpha$ pairs through their mutual $^{13}C\alpha$ or ^{15}N chemical shifts established in the amide or α proton-detected spectra, respectively, as depicted in Figure 3. Here,

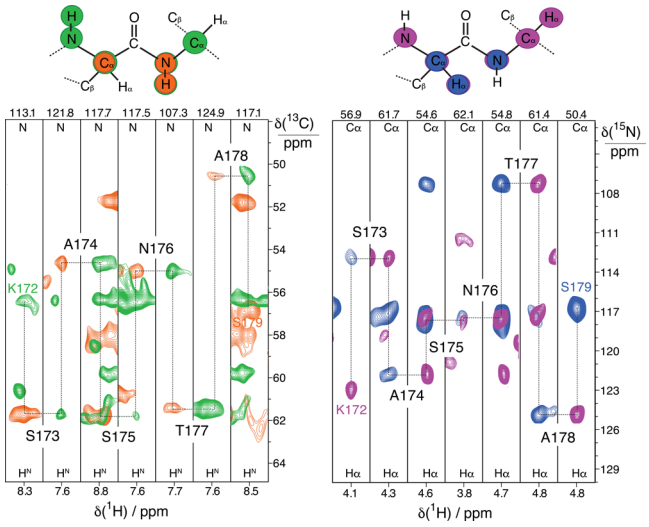

Figure 3. Sequential assignments of intensity correlations for residues 172−179 in fully protonated proteorhodopsin in lipids bilayers. 2D $^{1}H\alpha-^{13}C\alpha$ slices extracted from (H)CANH (green trace) and (H)(CO)CA(CO)NH (orange trace) spectra are shown in the left panel, and 2D $^{1}H-^{15}N$ slices from (H)NCAHA (magenta trace) and (H)N(CO)CAHA (blue trace) spectra in the right. The four spectra were acquired at 100 kHz MAS and 23.5 T.

representative portions of the four spectra that demonstrate sequential linking of amide and alpha pairs are reported. The choice of these pairs of experiments is motivated by the coherence lifetimes, which for membrane proteins are not as long as for microcrystalline samples. For comparison, while these 3D spectra were acquired in less than 2 weeks (Figure S1), $^{1}H^{N}$-detected experiments that rely on the faster decaying $^{13}C\alpha$ spins to enable $^{13}C'$- or $^{13}C\beta$-linking[25] have lower transfer efficiencies and significantly longer acquisition times. The $^{1}H\alpha-^{13}C\alpha$ and $^{1}H-^{15}N$ pairs also have roughly equal sensitivities, and the narrow dispersion in the $^{1}H\alpha$ dimension is offset by the narrow line width. This makes both types of spin pairs similarly useful in providing sequence-specific assignments. The backbone resonance assignments are further corroborated by analyses of the $^{13}C-^{13}C$-^{1}H TOCSY spectrum (Figure S4) that yields the assignment of the ^{1}H and ^{13}C side-chain resonances, thus enabling the identification of the amino acid types.

Resonance assignments for extensive portions of the proteorhodopsin backbone and side-chains were made based on spectra acquired at 100 kHz MAS. Despite the high degeneracy of aliphatic residues (32 Leu, 32 Ala, 24 Gly, 21 Val, and 19 Ile residues) that account for 49% of the proteorhodopsin sequence and the typically low chemical shift dispersions for helical proteins, the backbone resonances of 146 residues were sequence specifically assigned (Figure S5). Continuous linkages through 5 of the 6 proline residues were identified from analyses of $^{1}H\alpha$-detected 3D NMR correlation spectra. These residues are distributed in the transmembrane helices and extra-membrane loop regions. Importantly, resonance assignments were established for 57% of the ^{1}H and ^{13}C moieties of the aliphatic side-chains. The backbone chemical shifts clearly identify the seven transmembrane helices, connected by interhelical loops, and one additional short helix located in the extracellular E−F loop, in agreement with the structure of proteorhodopsin in detergents (Figure S6).

Such extensive resonance assignments facilitate the identification of inter-residue $^{1}H-^{1}H$ proximities that yield detailed site-specific information on proteorhodopsin structure in lipids. Key insights into the intra- and interhelical proximities between side-chains are obtained from analyses of high-resolution radio frequency-driven-recoupling (RFDR) spectra. For example, the 3D H(H)CH RFDR spectrum (1.4 ms mixing time, Figure 4) acquired from fully protonated proteorhodopsin shows numerous cross-signals that can be assigned to specific ^{1}H species using the resonance assignments established above. Subsequent analyses yield the identification of structural constraints, several of which are depicted schematically on the protein structure derived by solution NMR data, shown in Figure 4B. These include both intrahelical proximities, such as between the methyl ^{1}H of M134 and $^{1}H\alpha$ of G138 (Figure 4B, right, middle), and interhelical proximities, including the methyl ^{1}Hs of A116 and V182 (Figure 4B, right, bottom). These internuclear contacts within the transmembrane region are a direct way to probe the relative orientations of secondary structural elements. Especially important are the $^{1}H-^{1}H$ proximities of the $^{1}H\alpha$ of Gly residues and methyl groups, as these provide extremely useful structural constraints for α-helical proteins. In addition, the spectrum contains $^{1}H-^{1}H$ cross peaks between $^{1}H\alpha$ of Gly155 and two methyl groups with ^{1}H signals at 2.0 and 1.6 ppm, respectively, which are tentatively assigned to the retinal cofactor (Figure 4B, right, top). Such signals are valuable to establish the location, orientation and configuration of the chromophore in the transmembrane region of the protein, which is directly related to the protein functionality. In contrast, similar 3D spectra using perdeuterated and back-exchanged proteorhodopsin can only reveal $^{1}H^{N}-^{1}H^{N}$ contacts that primarily provide short- and medium-range intrahelical distance restraints. Importantly, much higher signal sensitivity and resolution were observed

DOI: 10.1021/jacs.7b05269
J. Am. Chem. Soc. 2017, 139, 13006−13012

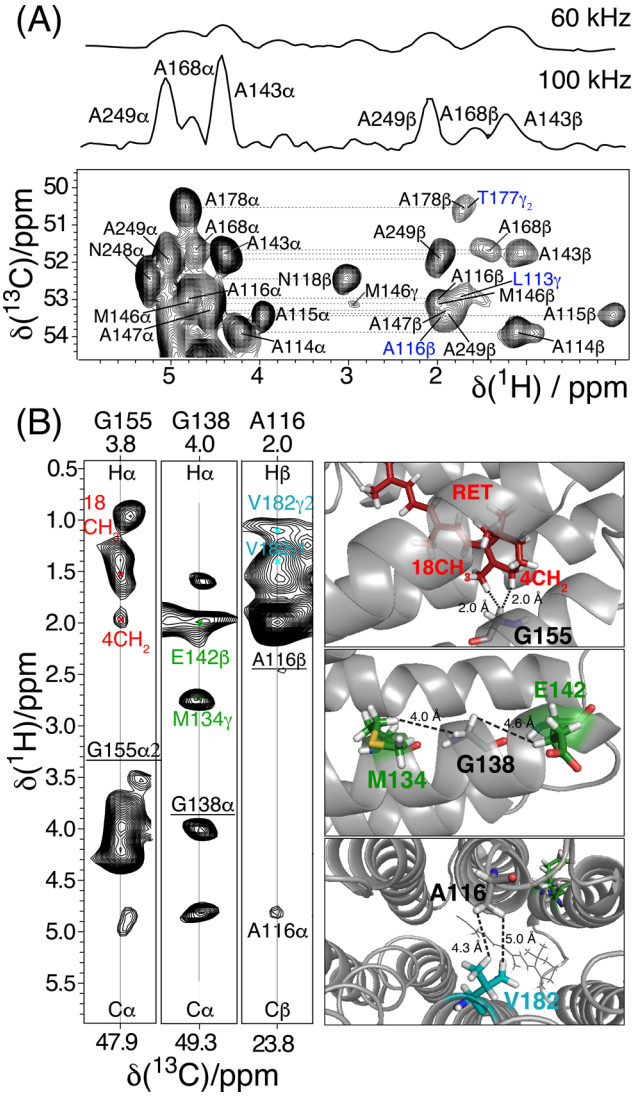

Figure 4. A) Alanine region of the 2D $^{1}H-^{13}C$ projection of a 3D H(H)CH RFDR spectrum acquired on U−[^{15}N,^{13}C] proteorhodopsin in lipids at 100 kHz MAS at 305 K and 23.5 T, using a 1.4 ms mixing time during which the RFDR rf-field was 200 kHz. Diagonal peaks are labeled in black and cross peaks in blue. Shown above the 2D projection are 1D ^{13}C slices extracted at the A249 C*α*−H*α* position (~51.9 ppm in the indirect dimension of the 2D projection) from the 3D RFDR spectrum acquired at 100 kHz and (up 60 kHz MAS. (B) 2D cross sections (left) of the 3D RFDR spectrum with $^{1}H-^{1}H$ correlations assigned to intra/interhelical and helix-retinal contacts cofactor, as depicted in the schematic 3D structure of the protein (right).

from the fully protonated sample at 100 kHz MAS versus an otherwise identical measurement at 60 kHz MAS on a 5-fold larger sample (Figure 4A).

The structures and properties of fully protonated membrane proteins in lipid bilayers are expected to closely resemble those in native cell-membrane environments. Interestingly, all of the $^{1}H-^{1}H$ contacts between the transmembrane helices reported above can be explained on the basis of the structure of proteorhodopsin in micellar (diheptanoyl-phosphocholine, diC_7PC) surfactant solution.[13] In combination with the ^{13}C chemical shift analysis above, this establishes that for the compositions and conditions investigated, the structures of proteorhodopsin in lipid bilayers and in micellar surfactant solution are very similar, and that even the position of the retinal cofactor within the transmembrane pocket is maintained. While in many cases solubilizing detergents have been observed to alter the structures or functionalities of membrane proteins,[26] that is not the case here. NMR structural analyses of fully protonated membrane proteins in lipids enabled by fast MAS represent an essential step to validating the conclusions from solution NMR data in detergent micelles.

From the present data, the oligomeric state of proteorhodopsin in lipid bilayers cannot be concluded, since it is not possible to identify any intermonomer cross peak in the 3D H(H)CH RFDR spectrum reflecting the presence of pentamers and/or hexamers. Unambiguous detection of such cross-peaks is extremely challenging due to the partial side chain assignment, the signal degeneracy, and the sample heterogeneity in terms of oligomeric composition. In order to identify such contacts, different strategies aimed at decreasing the sample heterogeneity and the spectral overlap and increasing the signal sensitivity can be adopted, such as the expression of mutants that stabilize a single oligomeric form to increase the sample homogeneity, or the use of tailored labeling schemes to decrease the spectral crowding, the acquisition of selective proton−proton distance restraints to increase the signal-to-noise, or the acquisition of 4D spectra with increased heteronuclear dimensionality to improve the spectral resolution.

CONCLUSIONS

Extensive atomic-level structural insights on a fully protonated membrane protein in native-like lipid environments are provided by ^{1}H-detected solid-state NMR spectra acquired under 100 kHz MAS conditions and at high (23.5 T) magnetic field. This approach yields highly resolved ^{1}H resonances from moieties throughout the protein, including those from transmembrane amide sites that are generally inaccessible to chemical exchange with water, and that are therefore absent in spectra of perdeuterated samples. This enables the sequential assignments of the protein resonances, including the majority of the aliphatic ^{1}H moieties, and notably the identification of long-range interhelical $^{1}H-^{1}H$ contacts between side-chains in transmembrane protein regions. To the best of our knowledge, this is the first report of long-range proximities between side-chain protons in a fully protonated membrane protein. Remarkably, this information was obtained with less than 0.5 mg of sample without the need for deuteration, thus circumventing a major roadblock to the structural characterization of membrane proteins by solid-state MAS NMR or other methods. This represents an important step toward the determination of membrane protein structures and their relationships to functional interactions in native-like lipid environments. The approach is expected to open opportunities to investigate a variety of complicated structure-dependent biochemical phenomena, including protein interactions in near-native environments or molecular recognition mechanisms that govern ligand binding to transmembrane receptors.

ASSOCIATED CONTENT

Supporting Information

The Supporting Information is available free of charge on the ACS Publications website at DOI: 10.1021/jacs.7b05269.

NMR coherence lifetimes and line widths. Diagrams with the NMR pulse sequence used. 2D $^{1}H-^{15}N$ CP−HSQC

DOI: 10.1021/jacs.7b05269
J. Am. Chem. Soc. 2017, 139, 13006−13012

NMR spectra acquired for U−[^{15}N, ^{13}C] PR in a 1.3 mm probe at 60 kHz and in a 0.7 mm probe at 100 kHz. ^{13}C−^{13}C 2D projection of the 3D (H)CCH-TOCSY spectrum. Topological plot of PR with the assigned residues and prediction of the secondary structure based on the analysis of the backbone chemical shifts. Probe considerations. Table of fully assigned ^{1}H, ^{13}C, and ^{15}N chemical shifts (PDF)

AUTHOR INFORMATION

Corresponding Authors

*bradc@engineering.ucsb.edu

*guido.pintacuda@ens-lyon.fr

ORCID

Bradley F. Chmelka: 0000-0002-4450-6949

Guido Pintacuda: 0000-0001-7757-2144

Present Address

[‖]Max-Plank Institute for Biophysical Chemistry, Am Fassberg 11, Göttingen, Germany.

Notes

The authors declare no competing financial interest.

ACKNOWLEDGMENTS

Financial support is acknowledged from the French CNRS (IR-RMN FR3050), from the European Research Council (ERC) under the European Union's Horizon 2020 Research and Innovation Programme (ERC-2015-CoG GA no. 648974), from the National Institutes of Health (R01GM116128), and from the USARO through the Institute for Collaborative Biotechnologies (grant W911NF-09-0001) and award W911NF-14-1-0617. L.B.A was supported by a MC incoming fellowships (REA grant agreement no. 624918 "MEM-MAS").

REFERENCES

(1) (a) Lange, A.; Giller, K.; Hornig, S.; Martin-Eauclaire, M. F.; Pongs, O.; Becker, S.; Baldus, M. *Nature* **2006**, *440*, 959−962. (b) Xu, J.; Durr, U. H.; Im, S. C.; Gan, Z.; Waskell, L.; Ramamoorthy, A. *Angew. Chem., Int. Ed.* **2008**, *47*, 7864−7867. (c) Etzkorn, M.; Kneuper, H.; Dunnwald, P.; Vijayan, V.; Kramer, J.; Griesinger, C.; Becker, S.; Unden, G.; Baldus, M. *Nat. Struct. Mol. Biol.* **2008**, *15*, 1031−1039. (d) Bajaj, V. S.; Mak-Jurkauskas, M. L.; Belenky, M.; Herzfeld, J.; Griffin, R. G. *Proc. Natl. Acad. Sci. U. S. A.* **2009**, *106*, 9244−9249. (e) Cady, S. D.; Schmidt-Rohr, K.; Wang, J.; Soto, C. S.; Degrado, W. F.; Hong, M. *Nature* **2010**, *463*, 689−692. (f) Sharma, M.; Yi, M.; Dong, H.; Qin, H.; Peterson, E.; Busath, D. D.; Zhou, H. X.; Cross, T. A. *Science* **2010**, *330*, 509−512. (g) Bhate, M. P.; McDermott, A. E. *Proc. Natl. Acad. Sci. U. S. A.* **2012**, *109*, 15265−15270. (h) Park, S. H.; Das, B. B.; Casagrande, F.; Tian, Y.; Nothnagel, H. J.; Chu, M.; Kiefer, H.; Maier, K.; De Angelis, A. A.; Marassi, F. M.; Opella, S. J. *Nature* **2012**, *491*, 779−783. (i) Shahid, S. A.; Bardiaux, B.; Franks, W. T.; Krabben, L.; Habeck, M.; van Rossum, B. J.; Linke, D. *Nat. Methods* **2012**, *9*, 1212−1217. (j) Wang, S.; Munro, R. A.; Shi, L.; Kawamura, I.; Okitsu, T.; Wada, A.; Kim, S. Y.; Jung, K. H.; Brown, L. S.; Ladizhansky, V. *Nat. Methods* **2013**, *10*, 1007−1012. (k) Wylie, B. J.; Bhate, M. P.; McDermott, A. E. *Proc. Natl. Acad. Sci. U. S. A.* **2014**, *111*, 185−190. (l) Andreas, L. B.; Reese, M.; Eddy, M. T.; Gelev, V.; Ni, Q. Z.; Miller, E. A.; Emsley, L.; Pintacuda, G.; Chou, J. J.; Griffin, R. G. *J. Am. Chem. Soc.* **2015**, *137*, 14877−14886. (m) Becker-Baldus, J.; Bamann, C.; Saxena, K.; Gustmann, H.; Brown, L. J.; Brown, R. C.; Reiter, C.; Bamberg, E.; Wachtveitl, J.; Schwalbe, H.; Glaubitz, C. *Proc. Natl. Acad. Sci. U. S. A.* **2015**, *112*, 9896−9901.

(2) Andreas, L. B.; Le Marchand, T.; Jaudzems, K.; Pintacuda, G. *J. Magn. Reson.* **2015**, *253*, 36−49.

(3) (a) Samoson, A.; Tuherm, T.; Gan, Z. *Solid State Nucl. Magn. Reson.* **2001**, *20*, 130−136. (b) Zhou, D. H.; Shea, J. J.; Nieuwkoop, A. J.; Franks, W. T.; Wylie, B. J.; Mullen, C.; Sandoz, D.; Rienstra, C. M. *Angew. Chem., Int. Ed.* **2007**, *46*, 8380−8383. (c) Marchetti, A.; Jehle, S.; Felletti, M.; Knight, M. J.; Wang, Y.; Xu, Z. Q.; Park, A. Y.; Otting, G.; Lesage, A.; Emsley, L.; Dixon, N. E.; Pintacuda, G. *Angew. Chem., Int. Ed.* **2012**, *51*, 10756−10759. (d) Vasa, S. K.; Rovo, P.; Giller, K.; Becker, S.; Linser, R. *Phys. Chem. Chem. Phys.* **2016**, *18*, 8359−8363.

(4) (a) Paulson, E. K.; Morcombe, C. R.; Gaponenko, V.; Dancheck, B.; Byrd, R. A.; Zilm, K. W. *J. Am. Chem. Soc.* **2003**, *125*, 15831−15836. (b) Chevelkov, V.; Rehbein, K.; Diehl, A.; Reif, B. *Angew. Chem., Int. Ed.* **2006**, *45*, 3878−3881.

(5) (a) Zhou, D. H.; Shah, G.; Cormos, M.; Mullen, C.; Sandoz, D.; Rienstra, C. M. *J. Am. Chem. Soc.* **2007**, *129*, 11791−11801. (b) Knight, M. J.; Webber, A. L.; Pell, A. J.; Guerry, P.; Barbet-Massin, E.; Bertini, I.; Felli, I. C.; Gonnelli, L.; Pierattelli, R.; Emsley, L.; Lesage, A.; Herrmann, T.; Pintacuda, G. *Angew. Chem., Int. Ed.* **2011**, *50*, 11697−11701. (c) Knight, M. J.; Pell, A. J.; Bertini, I.; Felli, I. C.; Gonnelli, L.; Pierattelli, R.; Herrmann, T.; Emsley, L.; Pintacuda, G. *Proc. Natl. Acad. Sci. U. S. A.* **2012**, *109*, 11095−11100. (d) Barbet-Massin, E.; Pell, A. J.; Retel, J. S.; Andreas, L. B.; Jaudzems, K.; Franks, W. T.; Nieuwkoop, A. J.; Hiller, M.; Higman, V.; Guerry, P.; Bertarello, A.; Knight, M. J.; Felletti, M.; Le Marchand, T.; Kotelovica, S.; Akopjana, I.; Tars, K.; Stoppini, M.; Bellotti, V.; Bolognesi, M.; Ricagno, S.; Chou, J. J.; Griffin, R. G.; Oschkinat, H.; Lesage, A.; Emsley, L.; Herrmann, T.; Pintacuda, G. *J. Am. Chem. Soc.* **2014**, *136*, 12489−12497. (e) Lamley, J. M.; Iuga, D.; Oster, C.; Sass, H. J.; Rogowski, M.; Oss, A.; Past, J.; Reinhold, A.; Grzesiek, S.; Samoson, A.; Lewandowski, J. R. *J. Am. Chem. Soc.* **2014**, *136*, 16800−16806. (f) Agarwal, V.; Penzel, S.; Szekely, K.; Cadalbert, R.; Testori, E.; Oss, A.; Past, J.; Samoson, A.; Ernst, M.; Bockmann, A.; Meier, B. H. *Angew. Chem., Int. Ed.* **2014**, *53*, 12253−12256. (g) Sinnige, T.; Daniels, M.; Baldus, M.; Weingarth, M. *J. Am. Chem. Soc.* **2014**, *136*, 4452−4455. (h) Mance, D.; Sinnige, T.; Kaplan, M.; Narasimhan, S.; Daniels, M.; Houben, K.; Baldus, M.; Weingarth, M. *Angew. Chem., Int. Ed.* **2015**, *54*, 15799−15803.

(6) Ward, M. E.; Shi, L.; Lake, E.; Krishnamurthy, S.; Hutchins, H.; Brown, L. S.; Ladizhansky, V. *J. Am. Chem. Soc.* **2011**, *133*, 17434−17443.

(7) (a) Zhou, D. H.; Nieuwkoop, A. J.; Berthold, D. A.; Comellas, G.; Sperling, L. J.; Tang, M.; Shah, G. J.; Brea, E. J.; Lemkau, L. R.; Rienstra, C. M. *J. Biomol. NMR* **2012**, *54*, 291−305. (b) Eddy, M. T.; Su, Y.; Silvers, R.; Andreas, L.; Clark, L.; Wagner, G.; Pintacuda, G.; Emsley, L.; Griffin, R. G. *J. Biomol. NMR* **2015**, *61*, 299−310.

(8) Medeiros-Silva, J.; Mance, D.; Daniels, M.; Jekhmane, S.; Houben, K.; Baldus, M.; Weingarth, M. *Angew. Chem., Int. Ed.* **2016**, *55*, 13606−13610.

(9) Nishiyama, Y. *Solid State Nucl. Magn. Reson.* **2016**, *78*, 24−36.

(10) Andreas, L. B.; Jaudzems, K.; Stanek, J.; Lalli, D.; Bertarello, A.; Le Marchand, T.; Cala-De Paepe, D.; Kotelovica, S.; Akopjana, I.; Knott, B.; Wegner, S.; Engelke, F.; Lesage, A.; Emsley, L.; Tars, K.; Herrmann, T.; Pintacuda, G. *Proc. Natl. Acad. Sci. U. S. A.* **2016**, *113*, 9187−9192.

(11) (a) Mroue, K. H.; Nishiyama, Y.; Kumar Pandey, M.; Gong, B.; McNerny, E.; Kohn, D. H.; Morris, M. D.; Ramamoorthy, A. *Sci. Rep.* **2015**, *5*, 11991. (b) Stanek, J.; Andreas, L. B.; Jaudzems, K.; Cala, D.; Lalli, D.; Bertarello, A.; Schubeis, T.; Akopjana, I.; Kotelovica, S.; Tars, K.; Pica, A.; Leone, S.; Picone, D.; Xu, Z. Q.; Dixon, N. E.; Martinez, D.; Berbon, M.; El Mammeri, N.; Noubhani, A.; Saupe, S.; Habenstein, B.; Loquet, A.; Pintacuda, G. *Angew. Chem., Int. Ed.* **2016**, *55*, 15504−15509.

(12) (a) Bamann, C.; Bamberg, E.; Wachtveitl, J.; Glaubitz, C. *Biochim. Biophys. Acta, Bioenerg.* **2014**, *1837*, 614−625. (b) Inoue, K.; Kato, Y.; Kandori, H. *Trends Microbiol.* **2015**, *23*, 91−98.

(13) Reckel, S.; Gottstein, D.; Stehle, J.; Lohr, F.; Verhoefen, M. K.; Takeda, M.; Silvers, R.; Kainosho, M.; Glaubitz, C.; Wachtveitl, J.; Bernhard, F.; Schwalbe, H.; Guntert, P.; Dotsch, V. *Angew. Chem., Int. Ed.* **2011**, *50*, 11942−11946.

DOI: 10.1021/jacs.7b05269
J. Am. Chem. Soc. 2017, 139, 13006−13012

(14) (a) Stone, K. M.; Voska, J.; Kinnebrew, M.; Pavlova, A.; Junk, M. J.; Han, S. *Biophys. J.* **2013**, *104*, 472−481. (b) Edwards, D. T.; Huber, T.; Hussain, S.; Stone, K. M.; Kinnebrew, M.; Kaminker, I.; Matalon, E.; Sherwin, M. S.; Goldfarb, D.; Han, S. *Structure* **2014**, *22*, 1677−1686. (c) Maciejko, J.; Mehler, M.; Kaur, J.; Lieblein, T.; Morgner, N.; Ouari, O.; Tordo, P.; Becker-Baldus, J.; Glaubitz, C. *J. Am. Chem. Soc.* **2015**, *137*, 9032−9043.
(15) (a) Shi, L.; Ahmed, M. A. M.; Zhang, W.; Whited, G.; Brown, L. S.; Ladizhansky, V. *J. Mol. Biol.* **2009**, *386*, 1078−1093. (b) Shi, L.; Lake, E. M.; Ahmed, M. A.; Brown, L. S.; Ladizhansky, V. *Biochim. Biophys. Acta, Biomembr.* **2009**, *1788*, 2563−2574.
(16) Bennett, A. E.; Rienstra, C. M.; Auger, M.; Lakshmi, K. V.; Griffin, R. G. *J. Chem. Phys.* **1995**, *103*, 6951−6958.
(17) Zhou, D. H.; Rienstra, C. M. *J. Magn. Reson.* **2008**, *192*, 167−172.
(18) (a) Good, D. B.; Wang, S.; Ward, M. E.; Struppe, J.; Brown, L. S.; Lewandowski, J. R.; Ladizhansky, V. *J. Am. Chem. Soc.* **2014**, *136*, 2833−2842. (b) Saurel, O.; Iordanov, I.; Nars, G.; Demange, P.; Le Marchand, T.; Andreas, L. B.; Pintacuda, G.; Milon, A. *J. Am. Chem. Soc.* **2017**, *139*, 1590−1597.
(19) Asami, S.; Szekely, K.; Schanda, P.; Meier, B. H.; Reif, B. *J. Biomol. NMR* **2012**, *54*, 155−168.
(20) Asami, S.; Schmieder, P.; Reif, B. *J. Am. Chem. Soc.* **2010**, *132*, 15133−15135.
(21) Huber, M.; Hiller, S.; Schanda, P.; Ernst, M.; Bockmann, A.; Verel, R.; Meier, B. H. *ChemPhysChem* **2011**, *12*, 915−918.
(22) Wang, S.; Parthasarathy, S.; Nishiyama, Y.; Endo, Y.; Nemoto, T.; Yamauchi, K.; Asakura, T.; Takeda, M.; Terauchi, T.; Kainosho, M.; Ishii, Y. *PLoS One* **2015**, *10*, e0122714.
(23) (a) Venters, R. A.; Farmer, B. T., II; Fierke, C. A.; Spicer, L. D. *J. Mol. Biol.* **1996**, *264*, 1101−1116. (b) Smith, A. A.; Ravotti, F.; Testori, E.; Cadalbert, R.; Ernst, M.; Bockmann, A.; Meier, B. H. *J. Biomol. NMR* **2017**, *67*, 109−119.
(24) Barbet-Massin, E.; Pell, A. J.; Jaudzems, K.; Franks, W. T.; Retel, J. S.; Kotelovica, S.; Akopjana, I.; Tars, K.; Emsley, L.; Oschkinat, H.; Lesage, A.; Pintacuda, G. *J. Biomol. NMR* **2013**, *56*, 379−386.
(25) Barbet-Massin, E.; Pell, A. J.; Knight, M. J.; Webber, A. L.; Felli, I. C.; Pierattelli, R.; Emsley, L.; Lesage, A.; Pintacuda, G. *ChemPhysChem* **2013**, *14*, 3131−3137.
(26) Cross, T. A.; Sharma, M.; Yi, M.; Zhou, H. X. *Trends Biochem. Sci.* **2011**, *36*, 117−125.

DOI: 10.1021/jacs.7b05269
J. Am. Chem. Soc. 2017, 139, 13006−13012